ACS Photonics

Article

pubs.acs.org/journal/apchd5

Influence of the Emission Layer Thickness on the Optoelectronic Properties of Solution Processed Organic Light-Emitting Diodes

Stefan Höfle, Tobias Lutz, Amos Egel, Felix Nickel, Siegfried W. Kettlitz, Guillaume Gomard, Uli Lemmer, and Alexander Colsmann*

Light Technology Institute, Karlsruhe Institute of Technology (KIT), Engesserstrasse 13, Karlsruhe 76131, Germany

ABSTRACT: We investigated the optoelectronic properties of solution processed organic light emitting diodes (OLEDs) as a function of their active layer thickness. By using a horizontal dipping technique and by accelerating the coating bar during wet film deposition, we fabricated OLED arrays with different emission layer thicknesses but identical process records in a single process step. The comparison of the optoelectronic device parameters allows for conclusions on injection limitation, the optimization of the layer thickness, and, in conjunction with optical simulations of the weak cavity effect, to promote a deeper understanding of the emission profile. To show the universality of this method, we investigated purely polymeric emitters, blends of polymers and small molecules as well as all-small molecule material systems.

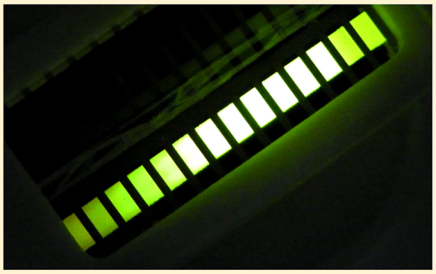

KEYWORDS: *organic light emitting diode, solution processing, material screening, optoelectronic performance, H-dipping*

Recent advances on the device efficiency and stability of organic light emitting diodes (OLEDs) have enforced their importance for the display industry and future lighting applications. Keys to the ongoing improvement of device performance are extensive material research, material screening, and the synthesis of new light emitting molecules. Usually, after synthesis, the performance potential of newly designed emitters and transport materials has to be investigated on the basis of a very limited amount of material. For an efficient light emission within the device, the optimum layer thickness of the material is of pivotal importance, since it influences both the electrical and optical device characteristics, for example, the charge carrier transport or the brightness and color of the OLEDs.[1−6] Comparing the performance of OLEDs with different active layer thicknesses can further elucidate whether the device performance is limited by injection or charge carrier transport.[7,8] The experimental optimization of layer thicknesses by common sample-by-sample fabrication and investigation is a time and material consuming work. Comprehensive optoelectronic device simulations are often considered as an alternative route to optimize device architectures. However, this approach requires knowledge of all optical and electrical material properties, as well as the exact location of the recombination zone within the emission layer,[9] hence, shifting the experimental efforts from device engineering to material property investigations. For vacuum processed OLEDs, an experimental screening process was introduced by C. Schmitz et al.,[10,11] who varied the emission layer thickness by using a movable mask during the evaporation of organic compounds onto an OLED array. For future low-cost devices, solution processing and printing of organic emitter materials is widely discussed. In the past, polymers were often considered the material class of choice due to their good film forming properties during solution deposition. Today, other materials such as metal oxides for electron or hole injection were introduced into the OLED technology.[12−21] Solution processing of materials with lower molecular weight (small molecules) is considered an interesting way forward to promising efficiencies and device stabilities, combining the advantages of both.[22,23] However, solution processed small molecule OLEDs often exhibit other optoelectronic properties than devices fabricated by vacuum deposition.[24]

Depending on the particular application, numerous functional layers from various material classes have to be optimized when designing new OLED architectures. In this work we present a feasible, fast, and material saving, though precise route to the experimental optimization of layer thicknesses in OLEDs. To demonstrate this powerful tool, we investigated various OLEDs comprising emission layers from either solution processed polymers, small molecules or polymer/small molecule blends, utilizing less than 4% of material as compared to conventional sample-by-sample device screening. Therefore, we solution deposited emission layers with varying thicknesses onto OLED arrays in a one-pass process. In order to change the layer thickness during the coating process, we adapted the horizontal dipping (H-dipping) method that has been used to produce uniform layers with constant thickness for organic light emitting diodes, thin-film transistors, and solar cells so far.[25−27] We have utilized this H-dipping technique for the fabrication of wedge-shaped active layers for organic lasers and organic solar cells before.[28−30]

Received: May 24, 2014
Published: September 3, 2014

EXPERIMENTAL SECTION

In order to investigate thickness dependent OLED properties, we designed an OLED array as depicted in Figure 1a. Each

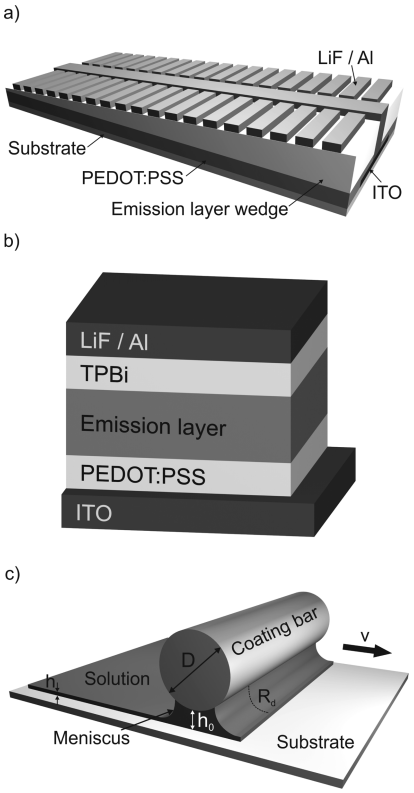

Figure 1. (a) Schematic of the OLED array: The hole injection layer PEDOT:PSS with constant layer thickness was deposited atop a structured ITO electrode. The subsequently deposited emission layer is wedge-shaped. The luminous areas with different layer thicknesses can be contacted via 2 × 19 cathodes and an anode busbar in the middle of the device. (b) OLED device architecture. The triplet exciton blocking TPBi was omitted for OLEDs comprising fluorescent Super Yellow layers. (c) Schematic of the horizontal dipping process including the relevant geometric parameters.

substrate carries two arrays of 19 OLEDs, both with steadily increasing active layer thickness. Indium tin oxide (ITO) coated glass substrates ($R_{\square} \approx 13\Omega/\square$) were structured in hydrochloric acid. The substrates were cleaned with acetone and isopropanol for 15 min in an ultrasonic bath. Afterward, the substrates were exposed to oxygen plasma for 2 min. Atop the ITO anode we deposited the OLEDs according to the device architecture in Figure 1b. All steps were carried out in a glovebox under a nitrogen atmosphere. A 25 nm poly(3,4-ethylenedioxythiophene):poly(4-styrenesulfonate) (PEDOT:PSS, Clevios P VPAI4083, Heraeus) hole injection layer was applied by doctor blading from a 1:3 ethanol diluted solution. Then the samples were annealed for 15 min at 130 °C. The polymeric emitter Super Yellow (Merck KGaA) was dissolved in toluene at a concentration of 4 mg/mL. To show the universality of this approach, we also investigated devices with small molecule emission layers. Therefore, 4,4′-*N*,*N*′-dicarbazole-biphenyl (CBP, Sensient Imaging Technologies) was used as a host for tris(2-phenylpyridine)iridium ($Ir(ppy)_3$, Sensient Imaging Technologies). CBP:$Ir(ppy)_3$ was mixed 10:1 by weight and dissolved in toluene at a concentration of 10 mg/mL. A total of 10 wt % of polystyrene was added in order to achieve homogeneous layers and to prevent crystallization.[22] Blue emitting devices comprised the host materials poly(vinyl carbazole) (PVK, Sigma-Aldrich) and 1,3-bis[(4-*tert*-butylphenyl)-1,3,4-oxadiazolyl]phenylene (OXD-7, Luminescence Technology Corp.) and the luminescent dye iridium(III)bis[(4,6-difluorophenyl)-pyridinato-N,C]picolinate (FIrpic, American Dye Source). PVK:OXD-7:FIrpic was mixed 7:3:1 by weight and dissolved in toluene at a concentration of 10 mg/mL. The emission layers were deposited via H-dipping utilizing a modified Zehntner ZAA 2300 doctor blading system, as illustrated in Figure 1c. A 90 μL aliquot of the respective solutions were fed into the 400 μm gap between substrate and the cylindrical coating bar with a diameter D = 10 mm. A wet film with varying thickness was deposited by moving the coating bar with increasing velocity v along the substrate that was heated up to 60 °C. For small capillary numbers ($C_a = \mu v/\sigma \ll 1$, where μ and σ represent the viscosity and the surface tension of the solution) and under the assumption of a Newtonian liquid, the final dry film thickness h can be calculated as follows:[25,27]

$$h = 1.43 \cdot v^{2/3} \cdot c_{mat} \quad (1)$$

$$c_{mat} = (\mu/\sigma)^{2/3} \cdot k \cdot R_d \approx \text{constant} \quad (2)$$

where k describes the film shrinking upon drying, R_d is the radius of the downstream solvent meniscus that is determined by the geometry of the system, that is, the radius of the coating bar $D/2$, the gap between coating bar and substrate h_0, and the distance between the meniscus edges at the bar. For devices comprising CBP:$Ir(ppy)_3$ and PVK:OXD-7:FIrpic, an additional 20 nm 1,3,5-tris(1-phenyl-1*H*-benzimidazol-2-yl)benzene (TPBi) hole blocking layer was thermally evaporated atop the light emitting layer in order to better confine the triplet excitons in the emission layer. A 0.7 nm lithium fluoride/200 nm aluminum (LiF/Al) top electrode was thermally evaporated. To reduce the device serial resistances, an additional aluminum busbar was evaporated on top of the ITO-anode. The OLED current density−voltage (J−V) characteristics were recorded with a source measurement unit (Keithley 238). The device luminous flux was recorded by a spectrum equipped with an integrating sphere. The spectrometer had been calibrated with a secondary standard calibration halogen lamp (Philips FEL-1000W). Current efficiencies (cd/A) and power efficiencies (lm/W) were calculated from the electrical and optical properties assuming lambertian light emission. Layer thicknesses were determined by a profiler (DektakXT, Bruker). We used the commercially available software SETFOS (Fluxim AG) to model the impact of the emitter layer thickness on both the current efficiency and the emission spectra of the Super Yellow OLED. We assumed dipole orientation parallel to the layer stack. To study the influence of the dipole location, we considered localized emission zones with a dipole-anode distance of 0.2, 0.4, 0.6, and 0.8 times the emission layer thickness. The cavity-free spectrum of Super Yellow was measured by photoluminescence of a thick Super Yellow layer on glass.

RESULTS AND DISCUSSION

In order to demonstrate the universality of our approach, we applied various emission layers on top of the PEDOT:PSS hole injection layer. Among other materials, we investigated the purely polymeric emitter Super Yellow and the blue-emitting

dx.doi.org/10.1021/ph500186m | ACS Photonics 2014, 1, 968−973

PVK:OXD-7:FIrpic hybrid, that is, a combination of polymers and small molecules. In the latter blend, the polymer matrix PVK ensures homogeneous deposition and layer formation from solution and at the same time good hole transport from the anode to the emitter molecule. We further examined state-of-the-art OLEDs comprising the well-investigated CBP:Ir-$(ppy)_3$ emitter system. By H-dipping, we applied all emission layers with thicknesses between 10 and 120 nm atop the OLED arrays, covering the entire range of typical emission layer thicknesses in OLEDs in one application process step. As depicted in Figure 2, the layer thicknesses increase linearly as a

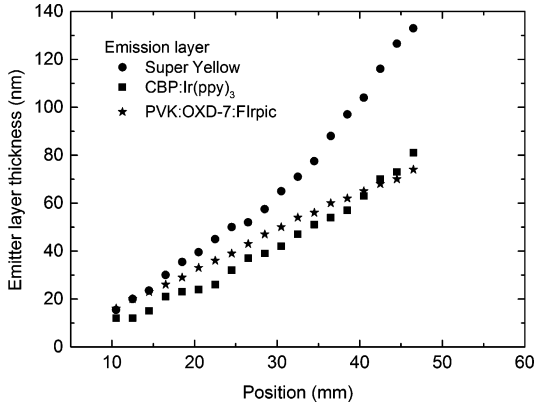

Figure 2. Emitter layer thicknesses vs the position on the substrate for the small molecule emitter (CBP:Ir$(ppy)_3$), the polymer emitter (Super Yellow), and the PVK:OXD-7:FIrpic blend. Each data point corresponds to one OLED of the array.

function of the position on the substrate. Whereas sample-by-sample device fabrication and characterization often lacks reproducibility, here, the accelerated coating bar provides an array of OLEDs fabricated from the very same process conditions with varying emission layer thickness. This excellent control of the H-dipping deposition process for all three material systems allows assessing the optoelectronic properties as a function of the layer thickness. Figure 3 summarizes important performance parameters of the OLEDs vs the emission layer thickness at a fixed device current density of 50 mA/cm^2. For all three material systems, the OLED driving voltages in Figure 3a increase upon increasing the emission layer thickness. To investigate the transport mechanisms, in Figure 3b, we plotted the average electrical field (by dividing the applied voltage minus the built-in voltage by the total thickness of all functional layers) that is required to drive the current through the device vs the emission layer thickness. Charge carrier injection into semiconductors can be described either by Fowler-Nordheim tunneling or by Richardson-Schottky thermionic emission.[31] Provided charge carrier injection limitation, Brütting et al. have shown that the device current density depends on the layer thickness if the electrical field is constant.[7,8] As we find a thickness independent electrical field at a constant device current density, we conclude that field dependent injection limitation controls the current in the OLEDs. While the charge carrier injection limits the electrical device performance, the optical device performance is predominantly ruled by quenching effects in the vicinity of the electrodes and by cavity effects. Quenching is particularly important for solution processed devices where the number of functional layers is often limited by the choice of solvents and, hence, buffer layers have to be discarded. Toward thinner

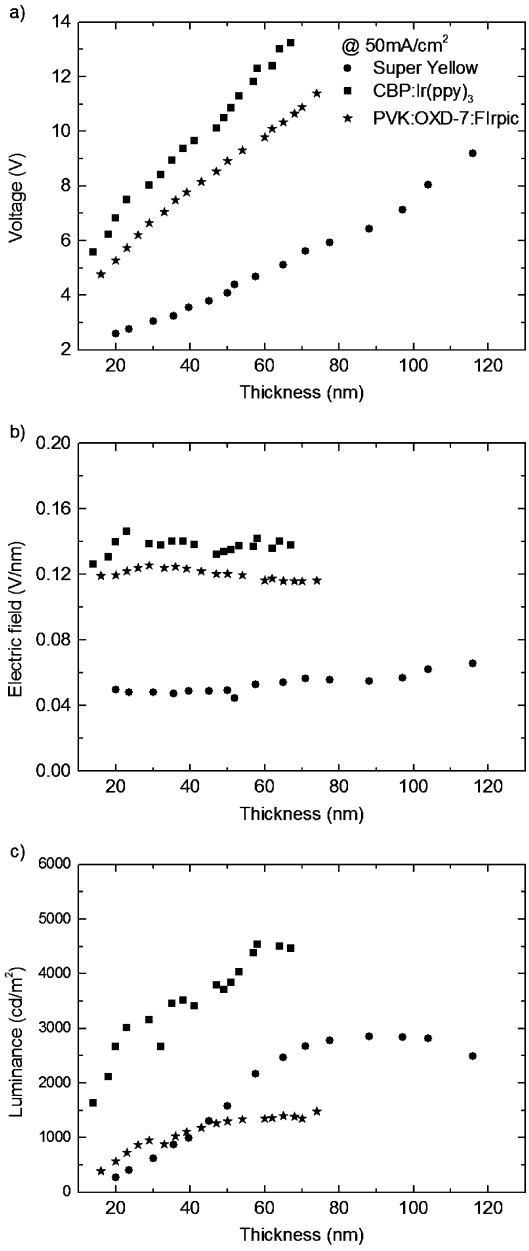

Figure 3. (a) At a constant current density of 50 mA/cm^2, the OLED driving voltage shifts toward higher voltages upon increasing the emission layer thickness. (b) At the same time, the electrical field shows no thickness dependency. (c) Luminance vs emission layer thickness.

layers, quenching becomes more pronounced because electrons and holes recombine closer to the electrode. For thin layers, we observed a strong decay in device luminescence for all three material systems, as exemplified in Figure 3c for an operation current density J = 50 mA/cm^2. We note that we also found some decay in luminescence toward thicker Super Yellow emission layers within the measurement interval, which we attribute to reduced extraction efficiencies due to photons coupled into waveguide modes within the device as discussed below. As a consequence of this interplay between electrical and optical device performance, we observed an optimum overall device performance in the intermediate layer thickness regime. Figure 4 shows the normalized device power efficiency as a function of the emission layer thickness for all three

dx.doi.org/10.1021/ph500186m | ACS Photonics 2014, 1, 968−973

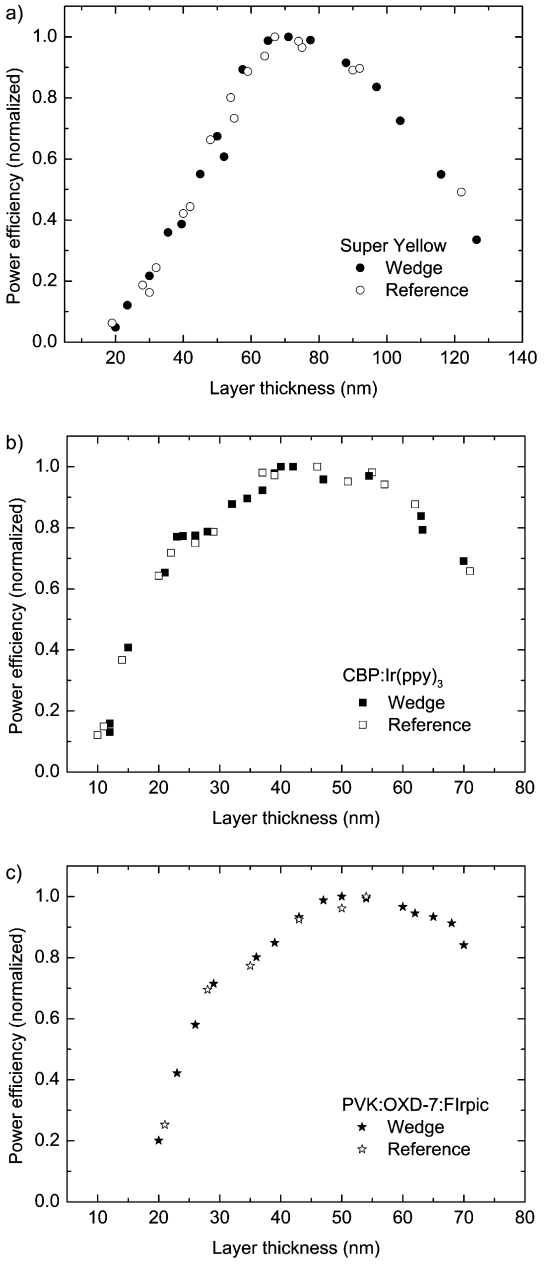

Figure 4. Normalized power efficiency as a function of the emission layer thickness for wedge shaped devices (black symbols) and reference OLEDs (open symbols). The latter were fabricated sample-by-sample. The emission layer comprises (a) Super Yellow, (b) CBP:Ir(ppy)$_3$, and (c) PVK:OXD-7:FIrpic. The power efficiency was determined at a constant luminance of (a) 2000 cd/m^2, (b) 2000 cd/m^2, and (c) 1500 cd/m^2.

emission material systems at a luminance of 2000 cd/m^2 (Super Yellow), 2000 cd/m^2 (CBP:Ir(ppy)$_3$), and 1500 cd/m^2 (PVK:OXD-7:FIrpic). The optimum emission layer thicknesses in this device setup are 60−80 nm (Super Yellow), 50−55 nm (PVK:OXD-7:FIrpic), or 40−50 nm (CBP:Ir(ppy)$_3$). We further compare the data from the OLED array (black symbols) with the efficiency of single reference OLEDs (open symbols) that were fabricated and investigated in a sample-by-sample approach where the emission layers were either spin-cast (Super Yellow) or H-dipped at a constant speed (PVK:OXD-7:FIrpic, CBP:Ir(ppy)$_3$). The optimum layer thicknesses for the reference OLEDs match the optimum layer thicknesses for the OLEDs of the array very well, nicely illustrating the feasibility of this layer thickness assessment in an OLED array.

In order to better understand this dependency of the current efficiency on the layer thickness, we simulated the optical loss mechanisms in the OLED devices. Henceforth, we deliberately focus on Super Yellow OLEDs. Considerations for the other two emitter systems can be done likewise. Besides the driving voltage that increases with an increasing layer thickness, optical losses are the predominant loss channels. Therefore, our optical device simulations take into account the absorption in the functional layers, the evanescent coupling into the metal cathode, that is, the excitation of surface plasmon polaritons (SPP), and the coupling into substrate and thin-film waveguide modes. For thin emission layers, the electroluminescence is inherently confined to a region near the cathode such that evanescent coupling to the cathode (plasmons) strongly limits the current efficiency (quenching). Toward thicker layers, the emission zone moves away from the cathode. At the same time, coupling into substrate modes and transverse electric (TE) waveguide modes becomes more relevant. Vanishing at reflecting surfaces, TE modes have a significant local density of states at positions away from the metal layer. An important input parameter for the simulation is the position of the emission zone within the emission layer.[32,33] In order to determine the position of the emission zone, we simulate the optical device properties as a function of the distance of the emission dipole from the anode.[34] The simulation results in Figure 5a show a strong influence of the dipole position on the thickness dependent current efficiency. When comparing the experimental data with the simulation results, we find the best match for a relative dipole position at 0.2 (where 0 refers to the anode interface and 1 to the cathode interface), indicating an emission close to the anode. In particular, the simulation resembles nicely the efficiency decay toward thin and thick emissions layers. To gain further insight into the optical loss mechanisms that limit the light outcoupling, we plot the relative contributions of the various loss channels in Figure 5b. For thin emission layers, we observe strong losses to SPP coupling that becomes negligible toward thicker absorber layers and, hence, an absolute emission zone position further away from the electrode. On the other hand, for thick emission layers, coupling into substrate and thin-film waveguide modes becomes the dominant loss channel. Consequently, the strongest outcoupling can be observed at an intermediate layer thickness of 80−100 nm, which again is in good agreement with the experimental data in Figure 5a. All optical loss mechanisms discussed here depend on the wavelength of the generated photons in the emission zone. As a consequence, the emission layer thickness affects the emission spectrum of the OLED. In Figure 5c, we compare the measured and simulated spectra of the Super Yellow OLED with emitter layer thicknesses of 24 and 116 nm, assuming an emission at 0.2 (relative position). While the OLED with the 24 nm emission layer exhibits a peak at a wavelength of $\lambda(d = 24\ \text{nm}) = 541$ nm, the emission spectrum broadens toward 116 nm emission layer thickness with a peak at $\lambda(d = 116\ \text{nm}) = 556$ nm. This translates into a CIE 1931 chromaticity shift from $(x,y) = (0.34, 0.57)$ at $d = 24$ nm to $(x,y) = (0.47, 0.52)$ at $d = 116$ nm. We found good agreement between the measured and simulated spectra, which confirms an emission near the Super Yellow−PEDOT:PSS interface.[35,36] For thin emission layers, we also observe a slight blue-shift of the spectrum in addition to the

dx.doi.org/10.1021/ph500186m | ACS Photonics 2014, 1, 968−973

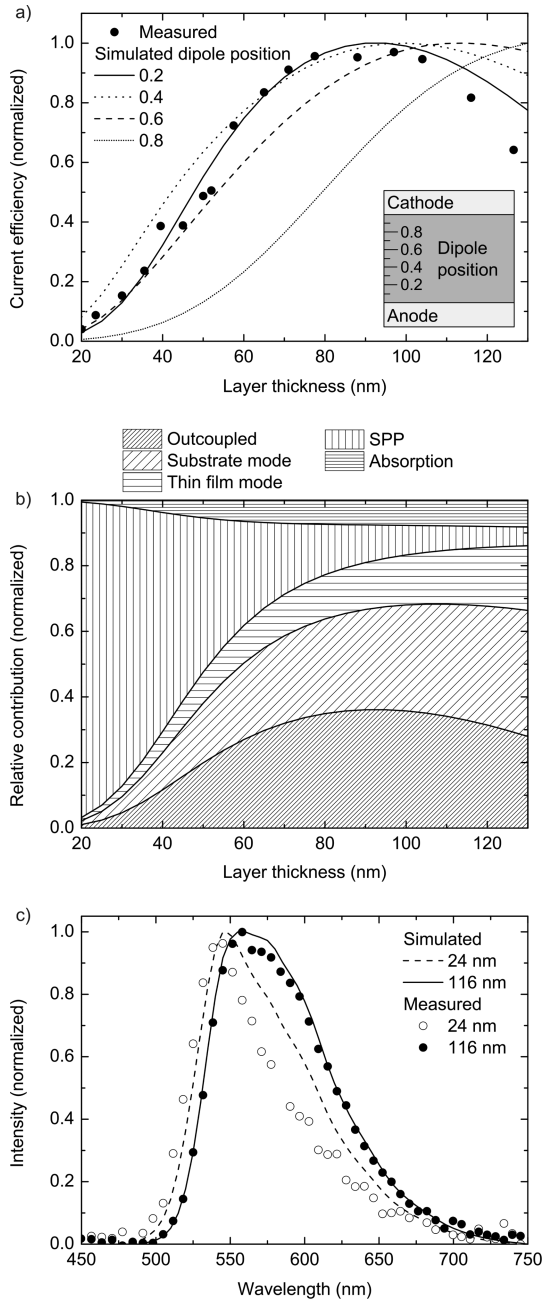

Figure 5. (a) Simulated and measured normalized current efficiencies of Super Yellow OLEDs vs the emitter layer thickness. In the simulation, a constant relative position of the dipole in the emitter layer was assumed for each curve. (b) Simulated waveguide analysis for different emission layer thicknesses. (c) Comparison of measured and simulated electroluminescense spectra for different emitter layer thicknesses. The dipole position for (b) and (c) was set at a 0.2 dipole−anode distance.

spectral narrowing. This blue-shift may be attributed to a strongly reduced lifetime of excited states due to near field coupling to the cathode. In Super Yellow, quenching can lead to a hampered relaxation of higher energy states, causing a blue shift of the fluorescence spectrum.[37]

In conclusion, we have presented a powerful tool to quickly assess the influence of the emission layer thickness on the optoelectronic OLED performance utilizing very small amounts of material, as exemplified on three material systems. The very good process control enables conclusions on the charge carrier injection or transport and allows for a fast identification of the optimum layer thickness.

AUTHOR INFORMATION

Corresponding Author

*E-mail: alexander.colsmann@kit.edu. Phone: +49 (0)721 60848587. Fax: +49 (0)721 60842590.

Notes

The authors declare no competing financial interest.

ACKNOWLEDGMENTS

The authors acknowledge funding by the Federal Ministry for Education and Research (BMBF) under Contract No. 13N11706 (Project MORPHEUS). S.H. thanks the Karlsruhe School of Optics and Photonics (KSOP) for support. G.G. acknowledges funding by the Alexander von Humboldt-Foundation. We acknowledge fruitful discussions with A. Arndt. C. Kaiser, and M. Klein provided the complex refractive indices of Super Yellow, PEDOT:PSS, and ITO for optical device simulations.

REFERENCES

(1) Huang, J.; Blochwitz-Nimoth, J.; Pfeiffer, M.; Leo, K. Influence of the thickness and doping of the emission layer on the performance of organic light-emitting diodes with PiN structure. *J. Appl. Phys.* **2003**, *93*, 838.

(2) Köhnen, A.; Irion, M.; Gather, M. C.; Rehmann, N.; Zacharias, P.; Meerholz, K. Highly color-stable solution-processed multilayer WOLEDs for lighting application. *J. Mater. Chem.* **2010**, *20*, 3301.

(3) Liu, T.-H.; Iou, C.-Y.; Wen, S.-W.; Chen, C. H. 4-(Dicyanomethylene)-2-*t*-butyl-6-(1,1,7,7-tetramethyljulolidyl-9-enyl)-4*H*-pyran doped red emitters in organic light-emitting devices. *Thin Solid Films* **2003**, *441*, 223.

(4) Bulović, V.; Khalfin, V.; Gu, G.; Burrows, P.; Garbuzov, D.; Forrest, S. Weak microcavity effects in organic light-emitting devices. *Phys. Rev. B: Condens. Matter Mater. Phys.* **1998**, *58*, 3730−3740.

(5) Watanabea, T.; Nakamuraa, K.; Kawamia, S.; Fukudaa, Y.; Tsujia, T.; Wakimotoa, T.; Miyaguchia, S.; Yahirob, M.; Yangb, M.-J.; Tsutsuib, T. Optimization of emitting efficiency in organic LED cells using Ir complex. *Synth. Met.* **2001**, *122*, 203.

(6) Yap, C. C.; Yahaya, M.; Salleh, M. M. Influence of thickness of functional layer on performance of organic salt-doped OLED with ITO/PVK:PBD:TBAPF6/Al structure. *Curr. Appl. Phys.* **2008**, *8*, 637.

(7) Brütting, W.; Berleb, S.; M, A. G. Device physics of organic light-emitting diodes based on molecular materials. *Org. Electron.* **2001**, *2*, 1.

(8) Crone, B. K.; Davids, P. S.; Campbell, I. H.; Smith, D. L. Device model investigation of single layer organic light emitting diodes. *J. Appl. Phys.* **1998**, *84*, 833.

(9) Lee, J.; Chopra, N.; So, F. Cavity effects on light extraction in organic light emitting devices. *Appl. Phys. Lett.* **2008**, *92*, 033303.

(10) Schmitz, C.; Posch, P.; Thelakkat, M.; Schmidt, H.-W. Efficient screening of electron transport material in multi-layer organic light emitting diodes by combinatorial methods. *Phys. Chem. Chem. Phys.* **1999**, *1*, 1777.

(11) Schmitz, C.; Pösch, P.; Thelakkat, M.; Schmidt, H.-W. Efficient screening of materials and fast optimization of vapor deposited OLED characteristics. *Macromol. Symp.* **2000**, *154*, 209.

(12) Höfle, S.; Do, H.; Mankel, E.; Pfaff, M.; Zhang, Z.; Bahro, D.; Mayer, T.; Jaegermann, W.; Gerthsen, D.; Feldmann, C.; Lemmer, U.; Colsmann, A. Molybdenum oxide anode buffer layers for solution processed, blue phosphorescent small molecule organic light emitting diodes. *Org. Electron.* **2013**, *14*, 1820.

(13) Höfle, S.; Bruns, M.; Strässle, S.; Feldmann, C.; Lemmer, U.; Colsmann, A. Tungsten oxide buffer layers fabricated in an inert sol-gel process at room-temperature for blue organic light-emitting diodes. *Adv. Mater.* **2013**, *25*, 4113.

(14) Murase, S.; Yang, Y. Solution processed MoO_3 interfacial layer for OPV prepared by a facile synthesis method. *Adv. Mater.* **2012**, *24*, 2459.
(15) Tan, Z.; Qian, D.; Zhang, W.; Li, L.; Ding, Y.; Xu, Q.; Wang, F.; Li, Y. Efficient and stable polymer solar cells with solution-processed molybdenum oxide interfacial layer. *J. Mater. Chem. A* **2013**, *1*, 657.
(16) Choi, H.; Kim, B.; Ko, M. J.; Lee, D.-K.; Kim, H.; Kim, S. H.; Kim, K. Solution processed WO_3 layer for the replacement of PEDOT-PSS layer in organic photovoltaic cells. *Org. Electron.* **2012**, *13*, 959.
(17) Meyer, J.; Hamwi, S.; Kröger, M.; Kowalsky, W.; Riedl, T.; Kahn, A. Transition metal oxides for organic electronics - energetics, device physics and applications. *Adv. Mater.* **2012**, *24*, 5408.
(18) Bolink, H. J.; Coronado, E.; Repetto, D.; Sessolo, M. Air stable hybrid organic-inorganic light emitting diodes using ZnO as the cathode. *Appl. Phys. Lett.* **2007**, *91*, 223501.
(19) Bolink, H. J.; Coronado, E.; Repetto, D.; Sessolo, M.; Barea, E. M.; Bisquert, J.; Garcia-Belmonte, G.; Prochazka, J.; Kavan, L. Inverted solution processable OLEDs using a metal oxide as an electron injection contact. *Adv. Funct. Mater.* **2008**, *18*, 145.
(20) Sessolo, M.; Bolink, H. J. Hybrid organic-inorganic light-emitting diodes. *Adv. Mater.* **2011**, *23*, 1829−45.
(21) Höfle, S.; Schienle, A.; Bruns, M.; Lemmer, U.; Colsmann, A. Enhanced electron injection into inverted polymer light-emitting diodes by combined solution-processed zinc oxide/polyethylenimine interlayers. *Adv. Mater.* **2014**, *26*, 2750.
(22) Höfle, S.; Pfaff, M.; Do, H.; Bernhard, C.; Gerthsen, D.; Lemmer, U.; Colsmann, A. Suppressing molecular aggregation in solution processed small molecule organic light emitting diodes. *Org. Electron.* **2014**, *15*, 337.
(23) Tekoglu, S.; Hernandez-Sosa, G.; Kluge, E.; Lemmer, U.; Mechau, N. Gravure printed flexible small-molecule organic light emitting diodes. *Org. Electron.* **2013**, *14*, 3493.
(24) Lee, T.-W.; Noh, T.; Shin, H.-W.; Kwon, O.; Park, J.-J.; Choi, B.-K.; Kim, M.-S.; Shin, D. W.; Kim, Y.-R. Characteristics of solution-processed small-molecule organic films and light-emitting diodes compared with their vacuum-deposited counterparts. *Adv. Funct. Mater.* **2009**, *19*, 1625.
(25) Park, B.; Han, M.-y. Organic light-emitting devices fabricated using a premetered coating process. *Opt. Express* **2009**, *17*, 21362.
(26) Park, B.; Jeon, H. G.; Choi, J.; Kim, Y. K.; Lim, J.; Jung, J.; Cho, S. Y.; Lee, C. High-performance organic thin-film transistors with polymer-blended small-molecular semiconductor films, fabricated using a pre-metered coating process. *J. Mater. Chem.* **2012**, *22*, 5641.
(27) Park, B.; Han, M.-y. Photovoltaic characteristics of polymer solar cells fabricated by pre-metered coating process. *Opt. Express* **2009**, *17*, 13830.
(28) Klinkhammer, S.; Liu, X.; Huska, K.; Shen, Y.; Vanderheiden, S.; Valouch, S.; Vannahme, C.; Bräse, S.; Mappes, T.; Lemmer, U. Continuously tunable solution-processed organic semiconductor DFB lasers pumped by laser diode. *Opt. Express* **2012**, *20*, 6357.
(29) Ge, C.; Lu, M.; Jian, X.; Tan, Y.; Cunningham, B. T. Large-area organic distributed feedback laser fabricated by nanoreplica molding and horizontal dipping. *Opt. Express* **2010**, *18*, 12980.
(30) Nickel, F.; Sprau, C.; Klein, M. F. G.; Kapetana, P.; Christ, N.; Liu, X.; Klinkhammer, S.; Lemmer, U.; Colsmann, A. Spatial mapping of photocurrents in organic solar cells comprising wedge-shaped absorber layers for an efficient material screening. *Sol. Energy Mater. Sol. Cells* **2012**, *104*, 18.
(31) Sze, S. S. M.; Ng, K. *Physics of Semiconductor Devices*; Wiley: New York, 1981.
(32) Nowy, S. Simulation based optimization of light-outcoupling in organic light-emitting diodes. *Proc. SPIE* **2009**, *7415*, 74151C.
(33) Meerheim, R.; Furno, M.; Hofmann, S.; Lussem, B.; Leo, K. Quantification of energy loss mechanisms in organic light-emitting diodes. *Appl. Phys. Lett.* **2010**, *97*, 253305.
(34) Burin, A. L.; Ratner, M. a. Exciton migration and cathode quenching in organic light emitting diodes. *J. Phys. Chem. A* **2000**, *104*, 4704.
(35) Gather, M. C.; Flämmich, M.; Danz, N.; Michaelis, D.; Meerholz, K. Measuring the profile of the emission zone in polymeric organic light-emitting diodes. *Appl. Phys. Lett.* **2009**, *94*, 263301.
(36) Flämmich, M.; Gather, M. C.; Danz, N.; Michaelis, D.; Bräuer, A. H.; Meerholz, K.; Tünnermann, A. Orientation of emissive dipoles in OLEDs: Quantitative in situ analysis. *Org. Electron.* **2010**, *11*, 1039.
(37) Im, C.; Lupton, J. M.; Schouwink, P.; Heun, S.; Becker, H.; Bassler, H. Fluorescence dynamics of phenyl-substituted polyphenylenevinylenetrinitrofluorenone blend systems. *J. Chem. Phys.* **2002**, *117*, 1395.